

Phenomenological and microscopic cluster models. II. Phase transitionsP. R. Fraser,¹ H. Yépez-Martínez,² P. O. Hess,¹ and G. Lévai³¹*Instituto de Ciencias Nucleares, UNAM, Circuito Exterior, C. U., A. P. 70-543, 04510 México, D. F., Mexico*²*Universidad Autónoma de la Ciudad de México, Prolongación San Isidro 151, Col. San Lorenzo Tezonco, Del. Iztapalapa, 09790 México D. F., Mexico*³*Institute of Nuclear Research of the Hungarian Academy of Sciences, Pf. 51, H-4001 Debrecen, Hungary*

(Received 17 August 2011; revised manuscript received 3 November 2011; published 18 January 2012)

Based on the results of a previous paper (Paper I), by performing the geometrical mapping via coherent states, phase transitions are investigated and compared within two algebraic cluster models. The difference between the semimicroscopic algebraic cluster model (SACM) and the phenomenological algebraic cluster model (PACM) is that the former strictly observes the Pauli exclusion principle between the nucleons of the individual clusters, while the latter ignores it. From the technical point of view the SACM is more involved mathematically, while the formalism of the PACM is closer to that of other algebraic models with different physical content. First- and second-order phase transitions are identified in both models, while in the SACM a critical line also appears. Analytical results are complemented with numerical studies on α -cluster states of the ^{20}Ne and ^{24}Mg nuclei.

DOI: [10.1103/PhysRevC.85.014317](https://doi.org/10.1103/PhysRevC.85.014317)

PACS number(s): 21.60.Fw, 21.60.Gx

I. INTRODUCTION

In a former contribution [1], called hereafter Paper I, we investigated the geometric mapping of the *phenomenological algebraic cluster model* (PACM) and the *semimicroscopic algebraic cluster model* (SACM) [2,3]. The first does not observe the Pauli exclusion principle while the second one does. The PACM belongs to the same family as models like the vibron model [4]. In both types of models we considered the same Hamiltonian, while the model space of each differs quite markedly. In the SACM the number of relative oscillation quanta is restricted from below, in accordance with the Wildermuth condition [5], while in the PACM the number of relative oscillation quanta starts from zero.

The method of geometrical mapping is from Ref. [6] for the SACM, which reduces to the usual one [7–10] when no Pauli exclusion principle is taken into account. We showed in Ref. [1] that the differences in the mapped geometrical potential are large. However, within the PACM one can reproduce the geometric potential of the SACM by including very complicated higher-order interactions.

In this paper we concentrate on the study of phase transitions. Phase transitions in nuclei and clusters of nuclei have been studied extensively. The most recent results in this field relevant for this contribution are Refs. [10–13]. The models and methods used can be found in Refs. [14,15], while a general introduction to *quantum phase transitions* can be found in Ref. [16]. We will show that not only second-order phase transitions but also first-order phase transitions may occur. Furthermore, in the SACM a critical line appears beyond which no phase transition occurs. Thus, the structure of the phase diagram of the SACM will be much richer.

We will also apply the mapping to two kind of systems, one with two spherical clusters and the other one with a deformed and a spherical cluster. Numerical studies are added. We will show that the PACM leads to inconsistencies when applied to real nuclei, while the SACM performs well. This study will be schematic. Though we will discuss definite cluster structures,

no numerical adjustment to spectral data is done. One can argue that it would be interesting to relate the discussion to real physical systems, for example, along an isotopic chain. As interesting and important this is, it would involve the fitting of a whole series of nuclei and it would deviate from the principle points we want to discuss. An investigations of this kind for cluster systems in the *sd* shell and of astrophysical interest are discussed in Ref. [17].

The paper is structured as follows: In Sec. II a general discussion on phase transition, both in the PACM and SACM, is given, independent of a particular system. In Sec. III, results are illustrated with two particular cluster systems, the α -cluster states of ^{20}Ne and ^{24}Mg . In the former, both clusters are spherical, while in the latter, one of them is deformed, leading to a more complex physical situation. Finally, in Sec. IV conclusions are drawn and a discussion is presented on the differences between the PACM and the SACM and their importance in the study of nuclear clusters.

II. PHASE TRANSITIONS IN ALGEBRAIC CLUSTER MODELS

In what follows we apply the formalism developed in Paper I [1] to discuss phase transitions in the SACM and PACM. Before that we present the general framework within which the discussion will be implemented.

A. Definition of a phase transition

Phase transitions are investigated using the following steps and the recommendations of [18–20]. This method can be applied to any system and does not depend on the notion of symmetries. This presentation does not need the language of catastrophe theory [21], which simplifies considerations.

- (i) In the first step the minima of the potential energy surface (PES) are determined in the space of the collective variables α_m . In the present case there is only one relevant variable α . This is due to the fact that

the distance vector between the clusters can always be aligned along the intrinsic z axis which connects the two clusters. The extrema are obtained from $\frac{dV}{d\alpha} = 0$. This determines the position of the extrema at $\bar{\alpha}_i$ ($i = 1, 2, \dots$) and the values $V(\bar{\alpha}_i)$ of the potential there. The $\bar{\alpha}_i$ are the values of the variable α at the i th minimum, which is a function of the interaction parameters $\vec{p} = (p_k)$, with p_k as a short-hand notation for the parameters $k = 1, 2, \dots, n_k$, with n_k being the number of parameters.

- (ii) Once the extrema are obtained, one determines *at each minimum* the first and second derivatives of the potential with respect to the parameters of the model, i.e.,

$$\frac{\partial^n V(\bar{\alpha}_i)}{\partial p_k^n}, n = 1, 2. \quad (1)$$

When we discuss the PACM and SACM further below, we will give first a general discussion on the properties of phase transitions, independent of the values of a particular subset of interaction parameters. In the subsequent concrete applications, however, we will fix most interaction parameters and vary only x and y , which control the transition from one effective symmetry [22] to another. This will give us particular curves in the space of phase transitions.

- (iii) The locations of phase transitions are determined by identifying the borders in the parameter space where at least two minima are at equal energy, i.e., $V(\bar{\alpha}_{i_1}) = V(\bar{\alpha}_{i_2})$ for some index values i_1 and i_2 of the minima. This results in a relation $f(p_1, \dots, p_{n_p}) = 0$ between the parameters, which allows one, in principle, to express one parameter in terms of the others.
- (iv) The phase transition is of order m when, up to $n = m - 1$, the derivatives of the potential with respect to the free parameters are equal at the point of phase transition, while the m th derivative of the potential, with respect to its parameters, is discontinuous at the point of the phase transition.

Note, again, that this procedure for determining the order of a phase transition is quite general and does not depend on identifying the phase with a dynamical symmetry. Thus, this procedure can also be applied to systems that do not exhibit dynamical symmetries.

B. Study of phase transitions in the SACM

Paper I [1] contains the general expression of the Hamiltonian (in Sec. II B) and the geometrically mapped SACM potential (in Sec. IV A). Here we recall only the essential formula, Eq. (17) of Paper I, necessary for the present discussion,

$$\begin{aligned} \langle H \rangle = & C(x, y) - (b + \bar{b})xy \left[A(x, y)\alpha^2 \frac{F_{11}(\alpha^2)}{F_{00}(\alpha^2)} \right. \\ & - B(x, y)\alpha^4 \frac{F_{22}(\alpha^2)}{F_{00}(\alpha^2)} + \alpha^6 \frac{F_{33}(\alpha^2)}{F_{00}(\alpha^2)} \\ & \left. - C(x, y)\alpha^2 \frac{F_{20}^{N-2}(\alpha^2)}{F_{00}(\alpha^2)} \right]. \end{aligned} \quad (2)$$

We also note that the $x = 0$ case relevant to the SO(4) to SO(3) phase transition has to be discussed separately. (See Eqs. (21) to (24) in Paper I [1].)

The complex structure of the geometrically mapped potential complicates an analytic treatment of the problem. It is, therefore, essential to formulate a set of criteria facilitating a straightforward way to determine the order of phase transitions.

The expression inside the parenthesis of Eq. (2) demonstrates that the explicit dependence of the potential on the parameters A , B , and C is linear of the type

$$\tilde{V} = \sum_k p_k \alpha^{m_k} f_k(\alpha), \quad (3)$$

with $m_k > 1$ and p_k being a short-hand notation for the k th parameter. The f_k are given by ratios of the functions $F_{pq}(\alpha)$ and are always greater than zero for $\alpha \neq 0$. Only the function F_{20}^{N-2} approaches zero for $\alpha \rightarrow \infty$. (See Eq. (27) in Paper I [1].)

According to the general discussion on phase transitions in Sec. II A, let us now turn to the potential minima located at $\bar{\alpha}_i$. We investigate their dependence on the parameters p_k , standing for A , B , and C . The structure of Eq. (3) guarantees that $\bar{\alpha}_1 = 0$ is always an extremum. Furthermore, not only its first-order derivatives but also the function value are zero at $\bar{\alpha}_1 = 0$. It is, thus, sufficient to focus on the second, deformed minimum, with $\bar{\alpha}_2$, for which the following consideration holds. There are two possibilities: (a) $\bar{\alpha}_2 > 0$ or (b) $\bar{\alpha}_2 = 0$. The consequences are seen by determining the first absolute derivative of the potential with respect to the parameter p_k . This first derivative is given by

$$\frac{d\tilde{V}}{dp_k} = \frac{\partial \tilde{V}}{\partial p_k} + \frac{\partial \tilde{V}}{\partial \bar{\alpha}_i} \frac{\partial \bar{\alpha}_i}{\partial p_k} = \frac{\partial \tilde{V}}{\partial p_k}, \quad (4)$$

because $\frac{\partial \tilde{V}}{\partial \bar{\alpha}_i}$ vanishes at the minimum. Taking into account Eq. (3), this is further expressed as

$$\frac{d\tilde{V}}{dp_k} = \bar{\alpha}_2^{m_k} f_k(\bar{\alpha}_2). \quad (5)$$

For case (a) this expression differs from zero (remember that $\bar{\alpha}_2 > 0$), while the derivative within the spherical minimum is equal to zero. In other words, there is a *first-order* phase transition.

For case (b), Eq. (5) is equal to zero, and, therefore, the phase transition must be of higher order. To determine which order, second-order derivatives are also needed,

$$\frac{d^2 \tilde{V}}{dp_k^2} = \frac{d}{dp_k} \left(\frac{\partial \tilde{V}}{\partial p_k} \right) = \frac{\partial \bar{\alpha}_2^{m_k}}{\partial p_k} f_k(\bar{\alpha}_2) + \bar{\alpha}_2^{m_k} \frac{\partial f_k(\bar{\alpha}_2)}{\partial \bar{\alpha}_2} \frac{\partial \bar{\alpha}_2}{\partial p_k}. \quad (6)$$

Here we used the fact that in Eq. (5) there is no explicit dependence in p_k left. Since in this case $\bar{\alpha}_2 = 0$, Eq. (6) reduces to

$$\frac{d^2 \tilde{V}}{dp_k^2} = \frac{\partial \bar{\alpha}_2^{m_k}}{\partial p_k} f_k(\bar{\alpha}_2). \quad (7)$$

As both the f_k functions and the partial derivatives differ from zero, so is Eq. (7) in general, i.e., the phase transition is of *second order* in case (b).

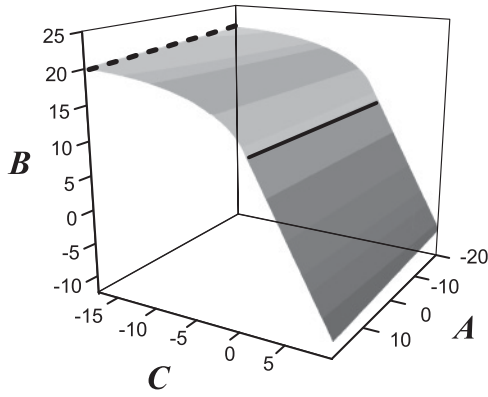


FIG. 1. The phase space diagram of the SACM as a function of the independent parameters A , B , and C . The solid line marks the change from a second- to a first-order phase transition and the dashed line denotes a “critical line.”

In conclusion, we have the simple identification of phase transitions: (a) When the deformed solution $\bar{\alpha}_2$, at the point of phase transition, differs from zero, then there is a *first-order* phase transition. (b) When the deformed solution $\bar{\alpha}_2$ is equal to zero, then there is a *second-order* phase transition. With the help of these results, we now can continue to discuss the general structure of the phase space within the SACM.

In Fig. 1 the surface where a phase transition takes place is plotted in the space of the independent parameters A , B , and C . The solid line marks a change from first-order to second-order transitions. For larger, positive C the transition is of second order, while for smaller, negative C it is of first order.

A remarkable finding is that at approximately $C \approx -15$ the surface of the phase transition ceases to exist. Beyond that point, no phase transition can be observed, i.e., the straight line at approximately $C \approx -15$ represents a *critical line*. This is shown by a dashed line in Fig. 1. One then can trace a straight line from below the surface, around the critical line, ending up above the surface without passing through a phase transition, which is similar to the critical point in the two-dimensional phase diagram of water. Fixing all interaction parameters except x and y (as we will do in the numerical applications), passing from one dynamical symmetry limit to another one will trace a line in this three-dimensional space. Depending on the fixed parameters, this line will or will not cross the surface of phase transition.

Figure 2 displays $\bar{\alpha}_2$ corresponding to the deformed solution at the point of phase transition as a function in A and C . (Remember that the *spherical solution* corresponds to the always existing extremum at $\alpha = 0$ in the case it is a local minimum.) Each point of the surface represents also a given B at which the phase transition occurs, i.e., B is fixed by the requirement that there is a phase transition. In this figure the solid line also represents the change from one type of phase transition to the other one. For larger, positive C $\bar{\alpha}_2 = 0$ holds, and it corresponds to a second-order phase transition. For smaller, negative C the $\bar{\alpha}_2 > 0$ holds at the point of phase transition, i.e., it corresponds to a first-order phase transition.

The *critical line* pointed out in Fig. 1 near $C \approx -15$ appears in Fig. 3 too. For a fixed A it corresponds to a *critical point*.

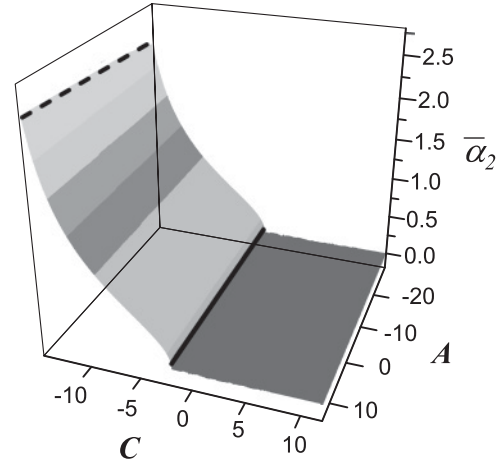


FIG. 2. The variable $\bar{\alpha}_2$ of the deformed solution, as a function in A and C . B is fixed by the requirement that one is at a point of a phase transition. The solid line marks the transition from a second- to a first-order phase transition and the dashed line denotes a “critical line.”

This critical point and the whole phase structure of the system is illustrated in Fig. 3, which corresponds to the fixed value $A = 10$. The solid line represents a cut through the phase transition surface. For $C > 0$ the phase transition is of second order, while for $C < 0$ is of first order. The roman numerals indicate the following regions: (1) Region I corresponds to the existence of two minima (one spherical and the other deformed), with the deformed one as the global minimum. (2) Region II also corresponds to two minima with the spherical as the global one. (3) In region III there is only one spherical minimum while (iv) in region IV there is only one deformed minimum. The region denoted by a zero refers to potential with no minimum. The other dashed lines do not indicate phase transitions; rather, they separate the areas where two minima exist and the ones where only one minimum exists. The line of phase transition ends at approximately $C \approx -15$.

The horizontal dotted line represents a division: Above this line the potential approaches a negative infinite value

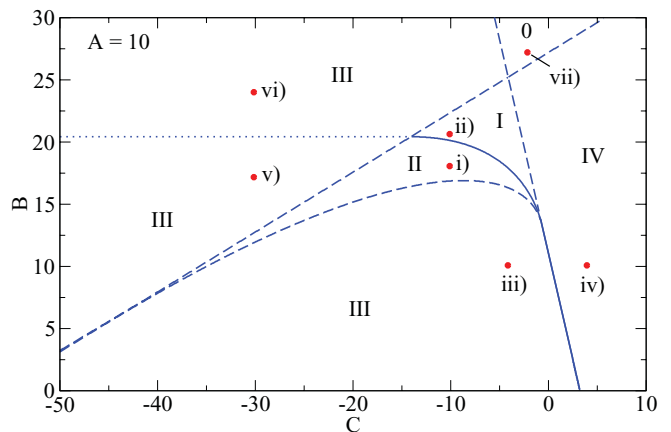


FIG. 3. (Color online) A cut through the phase space at $A = 10$. The notation is explained in the text.

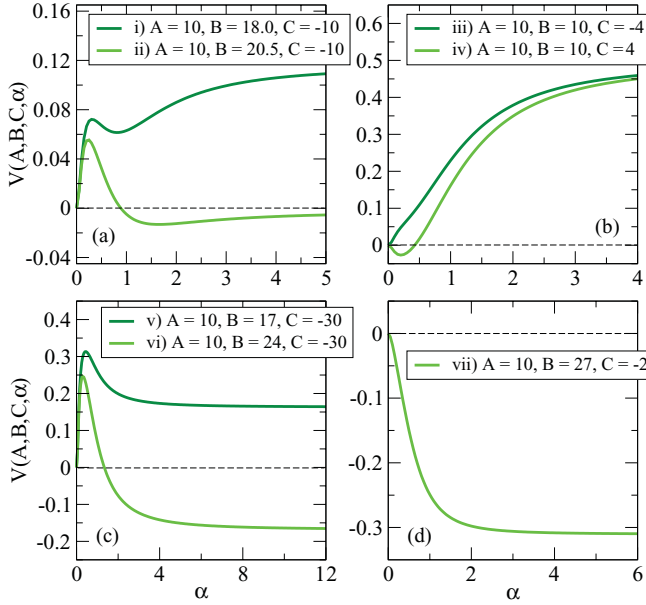


FIG. 4. (Color online) Several potentials for different values of B and C for $A = 10$ are shown. Some potentials approach a positive value, i.e., for $N \rightarrow \infty$ they approach to ∞ , while others approach to $-\infty$.

for $N \rightarrow \infty$, i.e., the potential gets unstable and the cluster system dissolves. Below that line the potential approaches plus infinity for $N \rightarrow \infty$, thus, the deformed solution corresponds to a stable cluster system.

Figure 4 gives a sample of energy functionals at a fixed N ($n_0 = 8$ and $N = 12$) in different regions, the specific points being denoted with lowercase letters in Fig. 3. The upper left panel shows functionals either side of the first-order phase transitions, points i) and ii). The upper right one shows graphs either side of the second-order phase transitions, points iii) and iv). The lower left panel shows a functional either side of the dotted line in the region III of greater B , points v) and vi), showing that while each have a barrier, one is bound as $\alpha \rightarrow \infty$ and the other is unbound. These tails are dependent on N , with the unbound approaching minus infinity and the bound plus infinity as $N \rightarrow \infty$. Thus, this region is unphysical. The fourth panel shows a fully unbound potential with no minima from region 0, point vii).

Note that the discussion of phase transitions is completely independent of the system considered, which is of great advantage. In the next section we will consider particular systems and study the properties of their phase transitions.

C. Study of phase transitions in the PACM

Here we apply the results obtained in Sec. IV B of Paper I [1]. We display only the expression of the normalized potential [Eq. (33) of Paper I]:

$$\tilde{V} = \{A\beta^2 - B\beta^4 + \beta^6\}. \quad (8)$$

We also remind the reader that the SO(4)-to-SO(3) transition needs a separate discussion, because in that case the potential

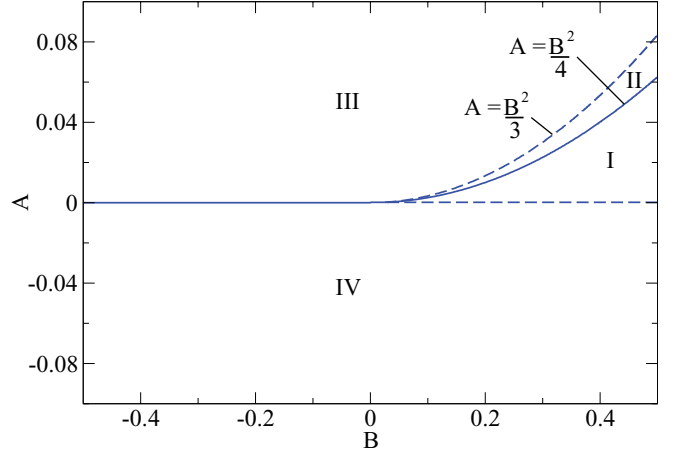


FIG. 5. (Color online) The parameter phase diagram for the PACM [23,24]. The horizontal axis is B , while the vertical axis corresponds to A . In region I and region II two minima exist, one spherical and one deformed. In region I the global minimum is the deformed one, while in region II it is the spherical minimum. In region III only a spherical minimum exists and in region IV the only minimum is a deformed one.

reduces to a quartic one. (See the discussion in Sec. IV B of Paper I [1].)

The simple form of the potential enables a simple curve analysis. There are, in general, two extrema,

$$\begin{aligned} \beta_1 &= 0 \\ \beta_2 &= \left\{ \frac{1}{3}(B \pm \sqrt{B^2 - 3A}) \right\}^{\frac{1}{2}}. \end{aligned} \quad (9)$$

The first solution, $\beta_1 = 0$, is always an extremum: Depending on the situation, it is a minimum or a maximum. The second solution is real only if $B^2 > 3A$ and $B > 0$ holds.

The structure of the phase space is depicted in Fig. 5. The horizontal line is the B axis while the vertical one is the A axis. On the left-hand side ($B < 0$) a spherical minimum exists for $A > 0$, while for $A < 0$ the minimum is deformed. The phase transition takes place at the line $A = 0$. For $B > 0$ and $A < 0$, a deformed minimum always exists. For $A > 0$ and below the dashed curve $A = B^2/3$ a deformed minimum coexists with a spherical minimum until $A = 0$ is reached. The solid curve is determined by requiring that the potential minima at β_1 and β_2 are degenerate, i.e., $\tilde{V}(\beta_1) = \tilde{V}(\beta_2)$, which leads to the condition $A = \frac{B^2}{4}$. Between the upper dashed and the solid curves the spherical minimum is the global one, while below the solid curve the global minimum is the deformed one. Crossing the solid line a phase transition takes place. It is of no surprise that the phase diagram in Fig. 5 is similar to Fig. 2 of Ref. [11].

III. NUMERICAL STUDIES

This section deals with two widely known cluster systems: ^{20}Ne as $^{16}\text{O} + \alpha$, where both clusters are spherical, and ^{24}Mg as $^{20}\text{Ne} + \alpha$, where one of them is deformed.

Since our aim is to study transitions from one particular dynamical symmetry limit to another one, we first fix all the

interaction parameters except x and y . The $\hbar\omega$ parameter was not adjusted but, rather, it was chosen according to the harmonic oscillator constant corresponding to the unified nucleus. The fixed interaction parameters are determined in such a way that in the dynamical symmetry limits the spectrum appears with the same scale as the physical measured one. The spectrum of the real nucleus would probably correspond to a single point in the (x, y) parameter space. However, our aim is not to reproduce the exact spectrum but rather to reach a conceptual understanding of phase transitions when going from one dynamical symmetry to another and to investigate the *hypothesis that a phase is defined by an effective symmetry*. One alternative method would be to adjust several cluster systems and to try to find a series of systems which, for example, would cross the surface of phase transitions at one point. We do not do this but instead postpone it for later consideration.

A. Two spherical clusters: $^{16}\text{O} + \alpha \rightarrow ^{20}\text{Ne}$

In this case the only degree of freedom is the radial motion, as the clusters do not have an internal structure apart from the fact that they are composed of fermions. Therefore, the cluster representation is $(\lambda_C, \mu_C) = (0, 0)$. As described in Paper I [1], the SO(3) limit does not exist as an independent limit in this case [the SO(3) Hamiltonian is a reduced version of the SU(3) Hamiltonian], so the $y = 1$ choice has to be made. The only transition to consider is, thus, between the SU(3) and the SO(4) limits.

Concerning the determination of the parameters, one has to take into account that some parameters appear in both dynamical symmetry limits, like γ preceding L^2 (see Eqs. (11) and (12) in Paper I [1]). We first determine the parameters in the SU(3) dynamical symmetry limit, which fixes γ , and then we determine the remaining parameter c , which appears in the SO(4) dynamical symmetry limit. The terms $\mathcal{C}_2(\lambda_C, \mu_C)$ and L_C^2 do not contribute to the Hamiltonian in this case, so the corresponding parameters are kept at zero. Note, that in this case $L_R^2 = L^2$.

1. The SACM

In the first step the parameters are adjusted within the SU(3) limit, setting $x = 1$ and $y = 1$ and in the SO(4) limit, setting $x = 0$ and $y = 1$. The parameters are depicted in Table I. The SACM yields reasonable results, because the ground-state band belongs to $n_\pi = 8$, $(\lambda, \mu) = (8, 0)$, where $n_\pi = 8$ corresponds to the minimal number of relative oscillation quanta n_0 required by the Wildermuth condition. The first excited 0^+ state corresponds to a $2\hbar\omega$ excitation and naturally lies at high energy as required by the experimental data. The spectra in the SO(4) and SU(3) limits are shown in the left and right extremes of the right panel, respectively, of Fig. 6. The spectrum of experimental ^{20}Ne states, each corresponding to this clusterization, is shown in the left panel. As already mentioned, the real nucleus will lie somewhere between $x = 1$ and $x = 0$, though, the spectrum at $x = 1$ is acceptable. In Ref. [17] the parameters of the Hamiltonian are adjusted to the

TABLE I. Parameter values defining the α - ^{16}O interaction. See Eq. (12) in Paper I [1].

		Hamiltonian					
a	\bar{a}	γ	a_{Clus}	\bar{b}	b		
-0.500	0.000	0.208	0.000	0.000	-0.009		
c	a_C	$a_R^{(1)}$	t				
0.250	0.000	0.000	0.000				
		Clusters					
λ_1	μ_1	$N_{0,1}$	β_1	λ_2	μ_2	$N_{0,2}$	β_2
0	0	0.00	0.00	0	0	0.00	0
		Quanta					
		$\hbar\omega$	n_0	N			
		13.2	8	12			

experimental spectrum and $B(E2)$ s were also calculated. In this calculation, the parameter $x = 1$ seems to be appropriate, too.

In order to see if a phase transition appears, and of which order it is, we added a curve to the (A, B, C) phase space in Fig. 7, depicting the transition from $x = 1$ to $x = 0$. The figure shows only the relevant part of the phase space, i.e., the one where the curve crosses the surface associated to the second-order phase transition. This occurs at approximately the $x = 0.6$ parameter value, which can also be appreciated in Fig. 6, where the density of states is largest at $x = 0.6$. In summary, the situation in this example corresponds to a phase transition of second order.

Figure 8 displays how the expectation value of n_π changes as the function of x . The lighter (orange online) and darker (red

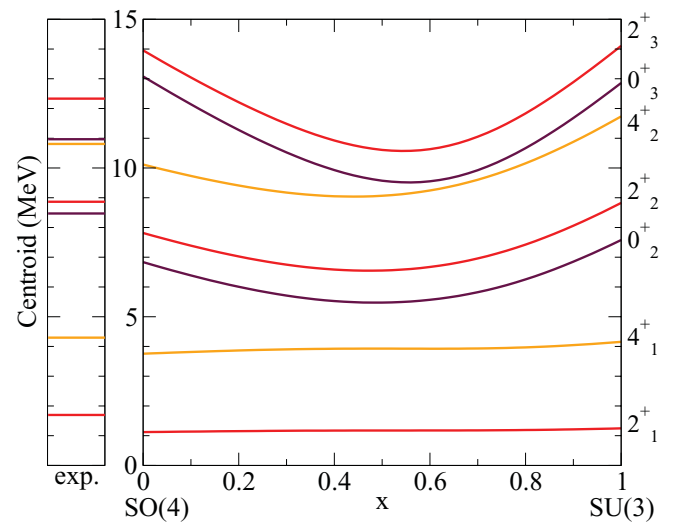


FIG. 6. (Color online) The lowest-energy states as the function of x for $^{16}\text{O} + \alpha \rightarrow ^{20}\text{Ne}$. The spins and parities are depicted in the legend. The light gray line corresponds to orange, the darkest gray line to purple, and the one in between to red. Lines with the same color indicate the same spin, as can be seen in the right side of the figure, where the lines start.

2. The PACM

This type of model was considered in Ref. [25], where a pure schematic investigation on possible phase transitions was presented. The model space was restricted to low n_π excitations. No parameter fit was applied to a physical system. We show here that the relation to a physical system is of utmost importance and can discriminate between physical and nonphysical models.

As a first step, we tried to adjust the parameters of the model in the SU(3) limit ($x = 1$ and $y = 1$) and in the SO(4) limit ($x = 0$ and $y = 1$). However, we already encountered severe problems in the SU(3) limit: The model space for even angular momentum starts with $n_\pi = 0$, thus, the lowest states are comprised of $n_\pi = 0$, $(\lambda, \mu) = (0, 0)$, which contains one $J^\pi = 0^+$ state, and $n_\pi = 2$, $(\lambda, \mu) = (2, 0)$, which contains a 0^+ state and a 2^+ state. The problems encountered are as follows.

- (i) Since the factor in front of L^2 has to be positive and supposing that the ground state belongs to $n_\pi = 0$ and the next excited positive parity state belongs to $n_\pi = 2$, the first excited 0^+ state will *always be lower* than the first excited 2^+ state. This contradicts the experimental spectrum with $E(2_1^+) = 1.634$ MeV and $E(0_2^+) = 8.7$.
- (ii) Since the 2_1^+ state belongs to a $2\hbar\omega$ excitation, with $\hbar\omega = 13.2$ MeV, the quadrupole-quadrupole interaction has to be unnaturally strong in order to shift the energy to 1.634 MeV. This, in turn, will move very high n_π excitations to low energy, even below the supposed ground state with $n_\pi = 0$.
- (iii) Due to the completely different SU(3) structure of the states within the ground-state “band,” one cannot talk about a rotation band.

Restricting the study to the SU(3) limit, the eigenvalues of the Hamiltonian are given by [15]

$$E = \hbar\omega n_\pi + (a - bn_\pi)n_\pi(n_\pi + 3) + \gamma L(L + 1). \quad (10)$$

Here we already see that for $\gamma > 0$ and a fixed n_π , higher spin states are higher in energy. In order to adjust the 2_1^+ and the 0_2^+ states to the experimental energies, the fitting routine assigns to both the ground state and the 2_1^+ state a *different* n_π . Using $N = 20$, as a result we obtain $n_\pi = 20$ (the total number of bosons was set to be 20) for the 0_1^+ and the 2_1^+ state, while the 0_2^+ state belongs to $n_\pi = 0$. When we change the total number of bosons, we get similar results. The mere fact that we have to involve states with $n_\pi = N$ indicates that no convergence is achieved, considering that N represents a cut-off value.

Similar results are also obtained when the SO(4) limit is considered. In the SO(4) limit, the energy is given by [15]

$$E = \frac{c}{4}(N - \omega)(N + \omega + 2) + \gamma L(L + 1), \quad (11)$$

where ω refers now to the SO(4) quantum number with $\omega = N, N - 2, \dots, 0$ or 1. The lowest state is normally taken as $\omega = N$, which contains $L = 0, 1, 2, \dots, N$ for even N and $L = 1, 2, 3, \dots, N$ for odd N . Thus, choosing $N = 20$, the ground-state band ($\omega = 20$) is composed of the angular-momentum states $L = 0, 1, 2, \dots, 20$ and the first excited band with even spin ($\omega = 18$) is given by the states $L = 0, 1, 2, \dots, 18$. Thus, the

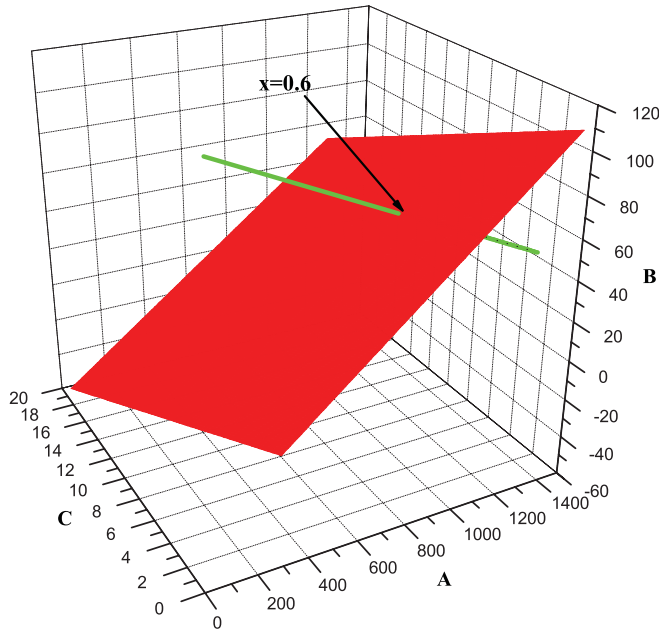


FIG. 7. (Color online) Part of the SACM phase space diagram, where the curve of the parameter values, as a function of x , crosses the surface of phase transition. The crossing occurs at approximately $x = 0.6$ and happens at the surface related to the second-order phase transition.

online) curves depict the result of the geometrical mapping and the numerical diagonalization, respectively. From $x = 1$ up to the point of phase transition, the effective SU(3) limit is realized and the expectation value is equal to the minimal number of π bosons, i.e., $n_0 = 8$. Below $x = 0.6$ the darker (red) curve begins to rise slightly, indicating that the structure of the system is changing.

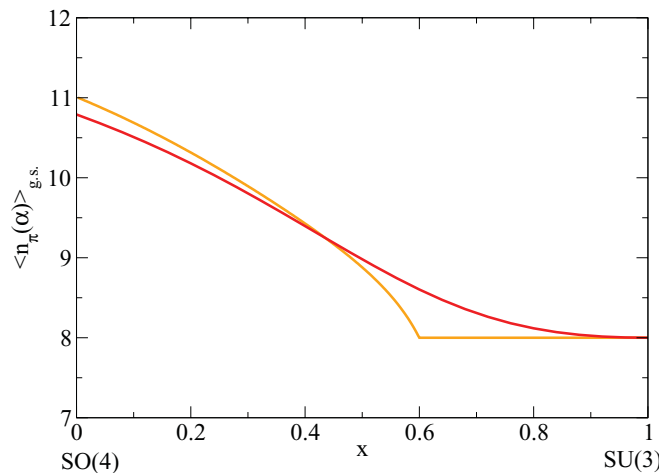


FIG. 8. (Color online) The expectation value of n_π (vertical axis) as the function of x . Starting from $x = 1$ the expectation value is 8, given by the lowest possible number of π quanta. From $x = 0.6$ on we observe a rise in the expectation value, reaching $n_\pi = 11$ at $x = 0$. The phase transition takes place at $x = 0.6$. The light gray (orange) line corresponds to the use of the coherent state, while the darker gray line (red) corresponds to the numerical calculation.

first excited 0^+ state can be set at higher energies than the first excited 2^+ state, adjusting the parameter c . Everything seems to be in order, except for the problems which the following discussion demonstrates.

The difference with respect to the SU(3) limit is that a SO(4) state is a mixture of many basis states in SU(3). We adjusted the spectrum of ^{20}Ne to the SO(4) limit and confirmed that for $L = 0$ the expectation value of the operator \mathbf{n}_π is given by [15]

$$\langle \mathbf{n}_\pi \rangle = \frac{N-1}{2}. \quad (12)$$

The problem here is that when the *cutoff* is increased, the structure of the states changes as $\langle \mathbf{n}_\pi \rangle$ increases, implying that no convergence has been reached. This also implies high shell excitations, *if* we assume that the two clusters are moving in a shell-model mean field, which has been proven in many microscopic calculations [26]. In the PACM, however, the mean field $\hbar\omega\mathbf{n}_\pi$ has no specific meaning, i.e., the parameter $\hbar\omega \rightarrow a_1$ can be very small. As shown above, the spectrum can be easily adjusted within the SO(4) limit. The fact that it adjusts the spectrum suggests that there must be some truth in it. Nevertheless, the basic degrees of freedom (clusters plus relative motion) cannot be interpreted as real clusters or relative motion, as is done in microscopic cluster studies, but must be in a complicated relation with them. Just what relations these are remains a big problem.

A possible solution to this problem is to redefine the pairing operator as $[(\pi^\dagger \cdot \pi^\dagger) - R^2(\sigma^\dagger)^2]$, i.e., the introduction of a new parameter R^2 which can be set proportional to $1/N$. In this way, the N dependence can be eliminated and physical results can be expected. This procedure was adopted in Ref. [27], where the vibron model was extended to three clusters describing the ^{12}C nucleus as an oblate symmetric top. Though, in Ref. [27] the SO(7) limit in a U(7) algebraic model, which describes three clusters, is considered, the same ideas can be translated here.

B. One spherical and one deformed cluster: $^{20}\text{Ne} + \alpha \rightarrow ^{24}\text{Mg}$

This is the first example where the cluster part has a structure due to the deformed ^{20}Ne .

1. The SACM

The fitting of the parameters in the SU(3) and SO(4) limit is performed in the same way as in the former case. The results are displayed in Table II.

Figures 9 and 10 display the expectation value of \mathbf{n}_π and the lowest states in energy, respectively, for all three transitions. The darker (red online) curve in Fig. 9 shows the results of the numerical diagonalization, while the lighter (orange online) curve shows the one of the geometrical mapping. The results are qualitatively similar to those encountered in the former example. The expectation value of \mathbf{n}_π starts in the SU(3) limit at 8 and increases towards the SO(4) limit. The transition is smooth in the numerical calculation, while in the geometrical mapping the transition is well pronounced. The transition is indicated by a sudden change in the slope

TABLE II. Parameter values for the α - ^{20}Ne interaction. See Eq. (12) in Paper I [1].

		Hamiltonian					
a	\bar{a}	γ	a_{clus}	\bar{b}	b		
-1.396	-0.136	0.197	0.000	-0.116	0.045		
c	a_c	$a_R^{(1)}$	t				
0.470	0.079	0.053	0.664	Clusters			
λ_1	μ_1	$N_{0,1}$	β_1	λ_2	μ_2	$N_{0,2}$	β_2
8	0	48.5	0.73	0	0	4.5	0
		Quanta					
		$\hbar\omega$	n_0	N			
		12.6	8	12			

at about $x = 0.25$ in the central panel of Fig. 9. The energy spectrum in Figure 10 does not show a particular structure at points of phase transition. Therein, the leftmost panel is again the experimental spectrum used, and the right three are theoretical results as x and y are adjusted. In the transition from SU(3) to SO(3) no phase transition appears, because the global minimum of the potential is always at $\alpha = 0$. One can observe a distinct behavior as a function of x and y between the states with positive and negative parity, marked as solid and dashed curves, respectively. The latter are more sensitive to the change in x and y .

Similar properties can be observed in the other limits, i.e., see the leftmost panel in Fig. 9. The energy spectrum also shows an accumulation of states at low energy at the point of phase transition at $x \approx 0.25$.

2. The PACM

Here we find similar inconsistencies with respect to the model space as in the case of ^{20}Ne in Sec. III A2. The cluster

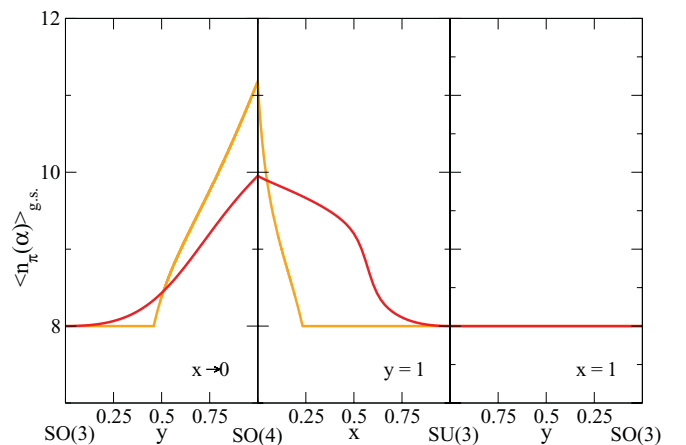


FIG. 9. (Color online) Expectation value of \mathbf{n}_π for the three transitions, (i) SU(3) to SO(4), (ii) SU(3) to SO(3), and (iii) SO(4) to SO(3). The light gray (orange) line corresponds to the use of the coherent state, while the darker gray (red) line corresponds to the numerical calculation.

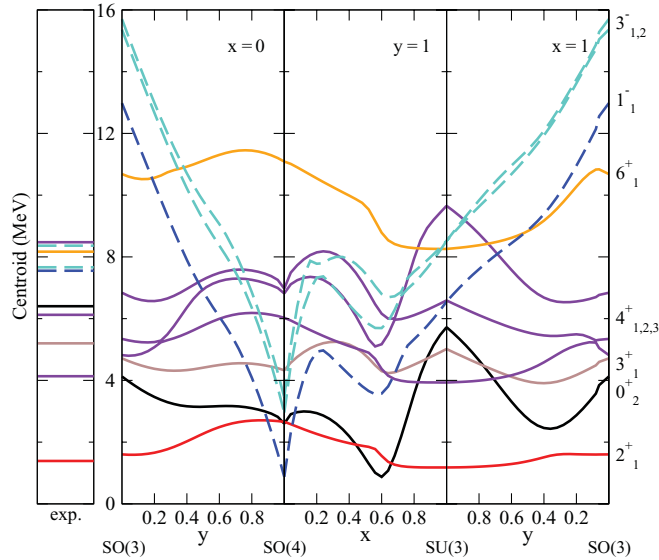


FIG. 10. (Color online) The lowest states in the three transitions, (i) SU(3) to SO(4), (ii) SU(3) to SO(3), and (iii) SO(4) to SO(3) for $^{20}\text{Ne} + \alpha \rightarrow ^{24}\text{Mg}$. The light gray line corresponds to orange, the darkest gray line to purple, and the one in between to red. Lines with the same color indicate the same spin, as can be appreciated on the right side of the figure, where the lines start.

irrep of ^{20}Ne is $(8,0)$, while the relative oscillation irreps are $(n_\pi, 0)$, with $n_\pi = 0, 1, 2, \dots$. Restricting to positive-parity states only, the lowest energy model space, in the SU(3) limit, consists of $(8, 0)$ at $0\hbar\omega$ and $(10,0)$ and $(6,2)$ for the $2\hbar\omega$ excitation. The ground-state band is a $(8,0)$ irrep and the next lowest 0^+ band (usually associated with $K = 2$) is the $(10,0)$ irrep at $2\hbar\omega$. Even if we change $\hbar\omega$ to an arbitrary small parameter a_1 , in order to bring the $2\hbar\omega$ states down in energy, the internal structure of the ground-state band is not what we expected, namely $(8,4)$. Also there is no $B(E2)$ transition between the ground-state band and the $K = 2$ band, because they belong to different irreps.

For the SO(4) limit one obtains a satisfactory fit, but again with the fact that the expectation value of the number operator n_π depends on the cutoff N .

IV. CONCLUSIONS

Phase transitions were investigated in two algebraic cluster models, one of which observed the Pauli exclusion principle between the nucleons of the individual clusters (SACM), while the other (PACM) did not. This analysis was based on the results of a previous work [1], in which the geometric

mapping of the two models had been performed using the coherent state formalism, leading to appropriate potential energy surfaces. The dynamical symmetries of the SACM and PACM had also been identified in Ref. [1], and in the present analysis special attention was paid to transitions between phases associated with the SU(3), SO(3), and SO(4) dynamical symmetries. The potential energy surfaces depend on the parameters appearing in the Hamiltonian shared by the SACM and PACM, including also the x and y variables controlling the transitions between the three dynamical symmetries. The phase space was reparameterized in terms of three parameters A , B , and C .

In the case of the PACM, the potential energy surface was a sextic oscillator in the intercluster distance variable, while for the SACM the potential shape was more complex due to the restrictions enforced by the Pauli principle. The potential energy surface typically contained up to two minima, one spherical and one deformed. The analysis identified both first- and second-order phase transitions for the PACM and the SACM, while in the latter case a critical line was also found.

The results were illustrated with numerical studies on the $^{16}\text{O} + \alpha$ and $^{20}\text{Ne} + \alpha$ systems, which correspond to two spherical clusters and to one spherical and one deformed cluster, respectively. The SU(3) limit was found to be the most appropriate one in reproducing the data of the cluster systems. Clear phase transitions were identified in the x parameter controlling the transition between the SU(3) and SO(4) limits. It was found that the PACM led to energy spectra that differ from the observed physical ones.

In the future it seems worthwhile to study many cluster systems of similar mass and investigate if there is a possibility that a chain of nuclei crosses a surface of phase transition. This should result in structural changes in the spectra and transition values. A first step in this direction will be published in Ref. [17].

ACKNOWLEDGMENTS

We gratefully acknowledge financial help from DGAPA-PAPIIT (Grant No. IN103212), from the National Research Council of Mexico (CONACyT), OTKA (Grant No. K72357), and from the MTA-CONACyT joint project. P.O.H. acknowledges very useful discussions with Octavio Castaños (ICN-UNAM), related to the differences in phase transitions in finite systems to the use of coherent states. Also useful discussions with Roelof Bijker (ICN-UNAM) are acknowledged, related to the definition of the radial distance. The authors are also thankful to József Cseh for illuminating discussions on the subject.

- [1] H. Yépez-Martínez, P. R. Fraser, P. O. Hess, and G. Lévai, *Phys. Rev. C* **85**, 014316 (2012).
 [2] J. Cseh, *Phys. Lett. B* **281**, 173 (1992).
 [3] J. Cseh and G. Lévai, *Ann. Phys. (NY)* **230**, 165 (1994).
 [4] F. Iachello, *Phys. Rev. C* **23**, 2778 (1981).

- [5] K. Wildermuth and Y. C. Tang, *A Unified Theory of the Nucleus* (Friedrich Vieweg & Sohn Verlagsgesellschaft mbH, Braunschweig, 1977).
 [6] P. O. Hess, G. Lévai, and J. Cseh, *Phys. Rev. C* **54**, 2345 (1996).

- [7] O. S. Roosmalen, Ph.D. thesis, Groningen, The Netherlands (1982).
- [8] O. S. Roosmalen and A. E. L. Dieperink, *Ann. Phys. (NY)* **139**, 198 (1982).
- [9] A. Leviatan and M. W. Kirson, *Ann. Phys. (NY)* **188**, 142 (1988).
- [10] P. Cejnar and J. Jolie, *Prog. Part. Nucl. Phys.* **62**, 210 (2009).
- [11] P. Cejnar and F. Iachello, *J. Phys. A* **40**, 581 (2007).
- [12] R. F. Casten, *Prog. Part. Nucl. Phys.* **62**, 183 (2009).
- [13] P. Cejnar, J. Jolie and R. F. Casten, *Rev. Mod. Phys.* **82**, 2155 (2010).
- [14] F. Iachello and R. D. Levine, *Algebraic Theory of Molecules* (Oxford University Press, Oxford, 1995).
- [15] A. Frank and P. Van Isacker, *Symmetry Methods in Molecules and Nuclei* (SyG editores, México D. F., 2005).
- [16] L. D. Carr, *Understanding Quantum Phase Transitions* (CRC Press, New York, 2011).
- [17] H. Yépez-Martínez, P. R. Fraser, and P. O. Hess, *J. Phys.: Conf. Series* **322**, 012010 (2011).
- [18] W. Greiner, L. Neise, and H. Stöcker, *Thermodynamics and Statistical Mechanics* (Springer, Heidelberg, 1995).
- [19] E. López-Moreno and O. Castaños, *Phys. Rev. C* **54**, 2374 (1996).
- [20] O. Castaños, R. López-Peña, J. G. Hirsch, and E. López-Moreno, *Phys. Rev. B* **74**, 104118 (2006).
- [21] R. Gilmore, *Catastrophe Theory for Scientists and Engineers* (Wiley, New York, 1981).
- [22] H. Yépez-Martínez, J. Cseh, and P. O. Hess, *Phys. Rev. C* **74**, 024319 (2006).
- [23] L. Parra Rodríguez, master's thesis, UNAM (2011).
- [24] P. R. Fraser, H. Yépez-Martínez, P. O. Hess, and L. Parra Rodríguez, *J. Phys.: Conf. Ser.* **322**, 012010 (2011).
- [25] Y. Zhang, Z.-F. Hou, H. Chen, H. Wei, and Y.-X. Liu, *Phys. Rev. C* **78**, 024314 (2008).
- [26] G. Rosensteel and J. P. Draayer, *Nucl. Phys. A* **436**, 445 (1985).
- [27] R. Bijker and F. Iachello, *Ann. Phys.* **298**, 334 (2002).